AGU PUBLICATIONS

JGR

Journal of Geophysical Research: Oceans

RESEARCH ARTICLE

10.1002/2014JC010175

Key Points:
- SODA is a useful tool for investigating large-scale ocean decadal variability
- Decadal patterns connect the Pacific and the Indian Ocean due to IPO changes
- The IPO extends through the upper 200–300 m to thermocline depths

Correspondence to:
J. M. Vargas-Hernandez,
jose.vargas.hernandez@una.cr

Citation:
Vargas-Hernandez, J. M., S. Wijffels, G. Meyers, and N. J. Holbrook (2014), Evaluating SODA for Indo-Pacific Ocean decadal climate variability studies, *J. Geophys. Res. Oceans*, *119*, doi:10.1002/2014JC010175.

Received 20 MAY 2014
Accepted 27 OCT 2014
Accepted article online 31 OCT 2014

Evaluating SODA for Indo-Pacific Ocean decadal climate variability studies

J. Mauro Vargas-Hernandez[1,2,3], Susan Wijffels[2,4], Gary Meyers[1,2], and Neil J. Holbrook[1,5]

[1]Institute for Marine and Antarctic Studies, University of Tasmania, Hobart, Tasmania, Australia, [2]CSIRO Oceans and Atmosphere Flagship, Hobart, Tasmania, Australia, [3]Laboratorio de Oceanografía y Manejo Costero, Universidad Nacional, Heredia, Costa Rica, [4]Centre for Australian Weather and Climate Research, Hobart, Tasmania, Australia, [5]ARC Centre of Excellence for Climate System Science, Hobart, Tasmania, Australia

Abstract Estimates of changes in upper ocean temperature, heat content, and sea level are dependent on the coverage of subsurface observations in space and time. Historically, these data are sparse, which has limited our understanding of ocean climate variability and change mechanisms. Ocean state estimates, which effectively represent a model synthesis and integration of the available observations, including internal observations in the ocean and surface forcing, help to address the inhomogeneity of sparse observations in space and time. Here we evaluate the representativeness of ocean state estimates from the Simple Ocean Data Assimilation Version 2.2.4 (SODA) data for studying Indo-Pacific Ocean decadal temperature and sea level variability over the period 1950–2007. The SODA data are evaluated against independent sea level anomalies from long-record tide gauges at Midway Island and Fremantle, reconstructed sea surface height anomalies, and sea surface height anomalies from TOPEX/Poseidon satellite altimeter observations at the decadal time scale. This study demonstrates that SODA captures the characteristic Interdecadal Pacific Oscillation (IPO) over the upper 200 m, and accurately represents these decadal changes against the independent observations. The SODA-product shows a meridional asymmetry of patterns that connect the western tropical Pacific and the Indian Ocean, apparently in relation to IPO changes. Regional sea level at the Midway Island and Fremantle tide gauges confirm this decadal connection and the relationship with the IPO. We concluded that SODA is potentially a useful tool to examine ocean decadal climate variability across the Indo-Pacific Ocean.

1. Introduction

Pacific decadal variability, characterized as either the Interdecadal Pacific Oscillation (IPO) or Pacific Decadal Oscillation (PDO), strongly influences a range of phenomena, including tropical rainfall [*Meinke et al*., 2005], fisheries [*Mantua et al*., 1997], and droughts (e.g., multidecadal drought frequency over the United States and Australia [*McCabe et al*., 2004; *Ummenhofer et al*., 2009]). As such there are potential benefits in obtaining accurate representations of decadal signatures in large-scale climate fields. Several studies have demonstrated the value of better understanding decadal ocean and climate variability. For instance, decadal variations of ENSO play an important role in the climate variability and potential predictability of, for example, agricultural yields and rainfall in Australia [*Power et al*., 1999a]. Furthermore, numerical ocean modeling research suggests that decadal ENSO acts to modulate the East Australian Current transports by incoming westward propagating oceanic Rossby waves [*Holbrook et al*., 2011]. These observational and modeling studies demonstrate the importance of having reliable data sets to study the linkage between ocean decadal variability and observed climate changes.

For oceanic data sets containing subsurface information, extracting unambiguous climate signatures can be particularly challenging, since historical profiles of the ocean's vertical structure are irregularly distributed in space and time across the globe. To address this, ocean state estimates from reanalysis data provide regularly gridded data based on model-assimilated observations with near-global coverage and long-term consistency. A key example is provided by the Simple Ocean Data Assimilation (SODA) [*Carton and Giese*, 2008]. Properly demonstrated, the utility of accurate ocean state estimates for the evaluation of ocean-climate model simulations on multidecadal times scales has obvious benefits. Robust reanalysis products are required to study decadal variability, since their signatures of physical variables (e.g., sea level, temperature

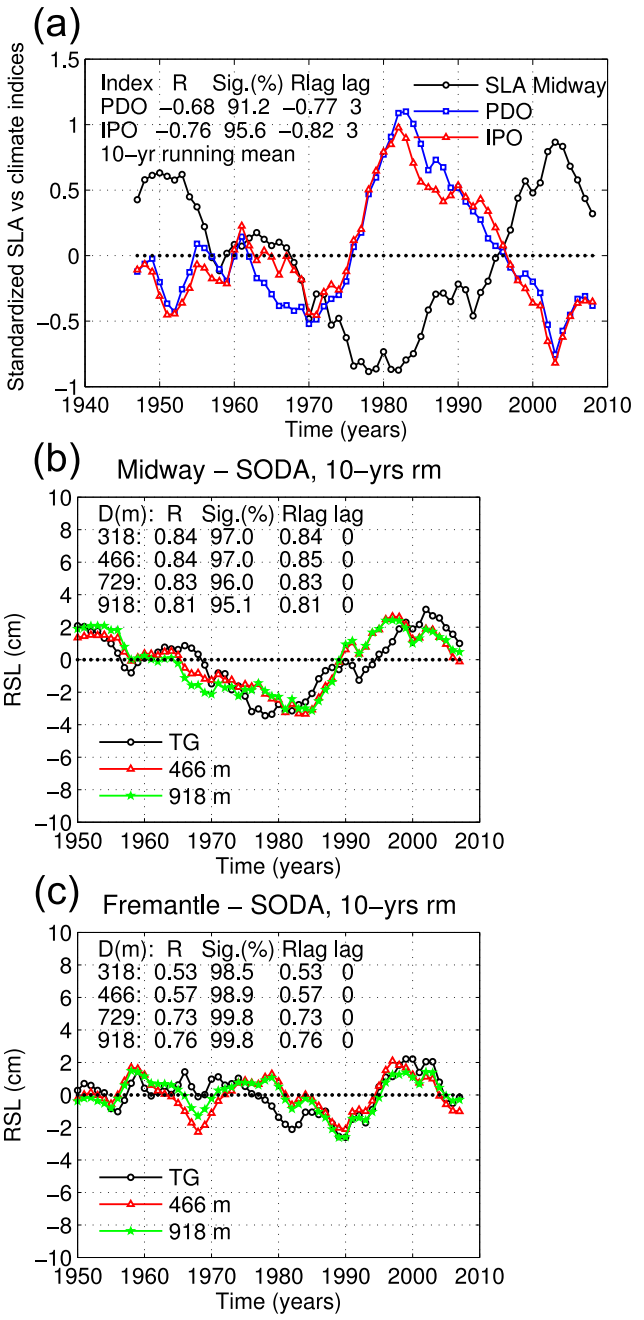

Figure 1. (a) Sea level anomalies observed at the Midway Island tide gauge and the PDO and IPO indices. A 10 year running mean is applied to the detrended and standardized time series in Figure 1a. Regional sea level (RSL) observed at the (b) Midway and (c) Fremantle tide gauges compared with SODA estimates for different depths, D (m). The steric sea surface height from SODA (Figures 1b and 1c) was integrated from the surface to four separate depths. The correlation coefficient (R), significance (Sig), cross-correlation coefficient (Rlag), and maximum lag in years are shown.

and ocean heat content) in the ocean tend to be smaller in magnitude than those on interannual time scales.

But how good is SODA for assessing decadal ocean climate variability? Of consideration is the fact that most reanalysis products incorporate mechanical bathythermograph (MBT) and expendable bathythermograph (XBT) profiles that are known to be affected by instrument biases, in particular the time-varying warm bias in XBTs [e.g., *Wijffels et al.*, 2008; *Levitus et al.*, 2009]. *Giese and Ray* [2011] have already shown that SODA captures well the decadal variability in El Niño in sea surface temperature (SST). But what about the subsurface? *Corre et al.* [2012] have further demonstrated the robustness of ocean reanalysis products to study decadal variability when compared with the World Ocean Database 2005, profiles from the Global Temperature-Salinity Profile Program, and similar data from the US-GODAE Argo Global Data Assembly Centre.

Sea level observations provide an independent data source for the evaluation of the SODA reanalysis product. Sea level accounts for the integrated effects of temperature and salinity as recorded in both in situ long-record tide gauge data and shorter record satellite remote sensed observations. Here we evaluate the decadal ocean climate variability described by SODA 2.2.4 against long record sea level observations from tide gauges (otherwise excluded, and therefore independent, from the reanalysis products) at two key locations. We also evaluate SODA in the Indo-Pacific using reconstructed sea-surface heights from *Church et al.* [2004], as well as sea surface heights from altimeter data for understanding decadal ocean climate variability and change.

The Midway and Fremantle tide gauges were chosen because they: (1) are among the longest tide gauge records available, (2) are representative locations for the oceanic characterization in sea level of the important decadal climate modes (e.g., IPO/PDO), (3) are sensitive to decadal variability in the Pacific and Indian Oceans, and (4) are representative of dynamic connections between the western tropical Pacific Ocean and the eastern South Indian Ocean via the equatorial and coastal waveguides. The Midway Island tide gauge

(Central North Pacific, 28°13′0.1194″N, 177°22′0.12″W) is a reliable long record (since 1947) and is close to the center-of-action of the PDO, with sea level there being strongly and significantly anticorrelated with the PDO and IPO indices (Figure 1a). The Fremantle tide gauge (southwest Western Australia, −32°3′56″S, 115°44′53″E) is the longest (since 1887) and most reliable record in the Indian Ocean, and its utility for studies of multidecadal sea level and ocean climate variability has been demonstrated in numerous previous studies [e.g., *Feng et al*., 2004, 2010]. These studies have shown that much of the low frequency variability observed at Fremantle is generated in the equatorial Pacific Ocean. In our evaluation presented here, we draw some conclusions about the utility of SODA for exploring ocean decadal variability in climate studies of temperature, sea level, and decadal ocean dynamics.

2. Data and Methods

Ocean state estimates from SODA 2.2.4 [*Carton and Giese*, 2008] are evaluated here. SODA applies an ocean model based on the Parallel Ocean Program (POP) version 2.0.1 numerics [*Smith et al*., 2010] to assimilate the observed data. Here we evaluate the utility of SODA in the Indo-Pacific Ocean sector for studies of decadal ocean climate variability. This data set is based on the monthly averaged values on the uniform 0.5° × 0.5° × 40-level grid spanning from 1871 to 2008 (at the date these data were downloaded). SODA includes the assimilation of all available hydrographic temperature and salinity observations [*Boyer et al*., 2009] and SST observations [*Woodruff et al*., 2010]. The model is driven by surface-wind stress from the second version of the Twentieth Century Reanalysis (20Crv2) Project [*Compo et al*., 2011] and SODA 2.2.4 includes the *Levitus et al*. [2009] corrections for XBT and MBT biases.

Sea surface height (SSH and its anomalies SSHA) is an important geophysical field in this study and we have used three estimates from different sources: steric SSHA from SODA (SodSSHA), reconstructed SSHA from *Church et al*. [2004] (RecSSHA), and SSHA from TOPEX/Poseidon satellite-altimeter data (AltSSHA).

Long record sea level data from the tide gauges at Midway Island (1947–2009) and Fremantle (1887–2009), provided by CSIRO Marine and Atmospheric Research (http://www.cmar.csiro.au/sealevel/index.html), were selected for the evaluation of the integrity of SODA in capturing decadal to multidecadal sea level variations directly observed. An approximated steric component of the sea level from the tide gauge data was calculated by removing the eustatic component to facilitate direct comparison with the steric SSH data derived from SODA. Here global mean sea level has been subtracted from the total sea level measured at the tide gauges in order to remove the eustatic component and thus leave only a residual that is close to the steric component (hereafter regional sea level). This approach assumes that the eustatic sea level contribution is homogeneous on decadal time scales. The sea level data from the tide gauges have also been corrected for Glacial Isostatic Adjustment (GIA) [*Davis and Mitrovica*, 1996; *Milne et al*., 2001]. The GIA values for the Midway Island and Fremantle tide gauges, respectively, of −0.15 and −0.37 mm/yr were subtracted from the sea level time series. A 10 year running mean filter was finally applied to the detrended data to characterize the decadal signature in the time series.

A lagged-correlation analysis between the sea level from two tide gauges and SodSSHA for a time-lag sequence from −10 to 10 years was carried out to evaluate whether SODA accurately tracks known decadal patterns (for example, IPO patterns in SST as described by *Folland et al*. [1999] and *Power et al*. [1999b]) in space and time across the Indo-Pacific Ocean. The steric SodSSHA (hereafter SodSSHA) were estimated by deriving the dynamic height anomaly across the 5–918 m depth range and dividing it by the gravitational acceleration. The time series of regional sea level at the Midway Island and Fremantle tide gauges were lag-correlated with the time series of SodSSHA at each spatial point in the Indo-Pacific Ocean for the period 1950–2007.

A similar analysis to that described above was performed by correlating SodSSHA and temperature anomalies from SODA with the IPO index in order to examine the ocean sea level and temperature response to the IPO throughout the Indo-Pacific Ocean. Here all the lagged-correlation analyses were applied to the 10 year running mean filtered and detrended data.

In addition to the above correlation analysis, we applied robust linear regression analysis, based on iteratively reweighted least squares, to estimate the response of temperature in SODA to the IPO. Maps of the regression coefficient were produced to identify the magnitude of response in different regions. We also

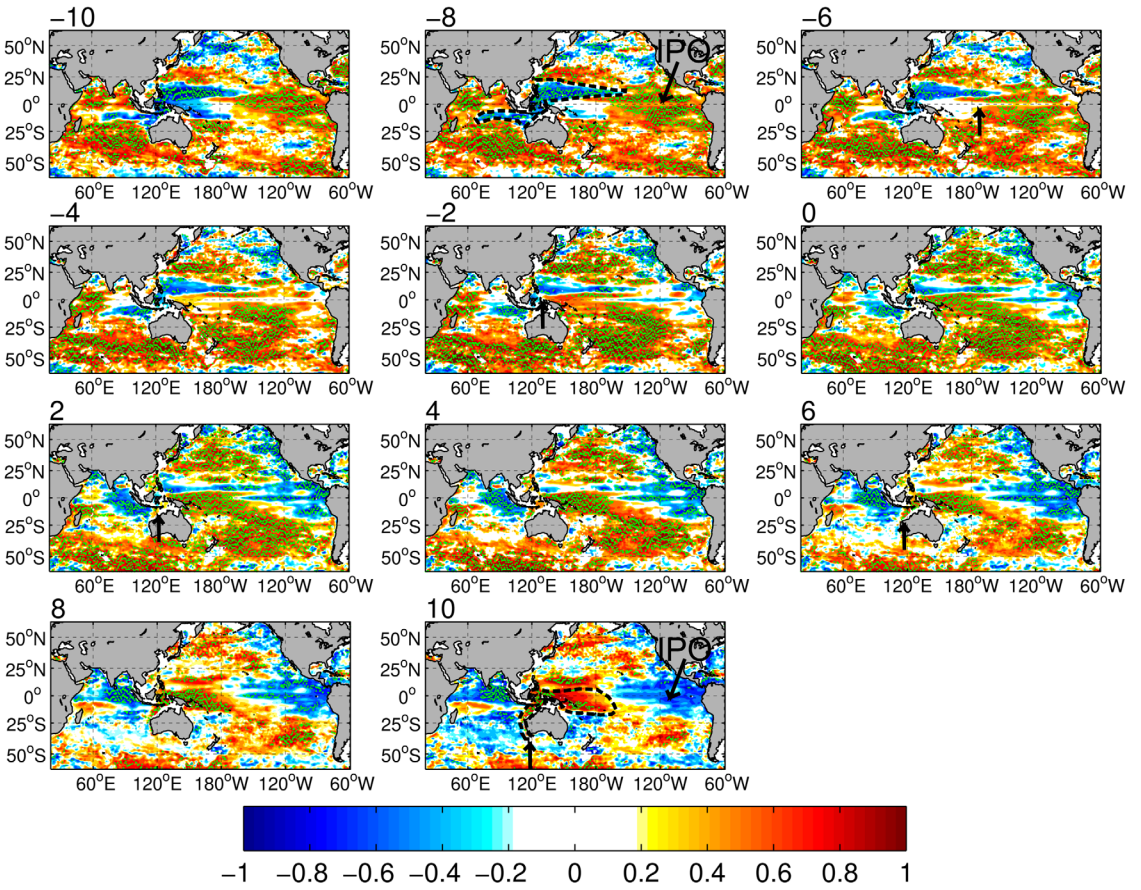

Figure 2. Spatial distribution of lagged-correlation coefficients (R) between regional sea level at Midway Island tide gauge and sea surface heights anomalies from SODA (SodSSHA) in the Indo-Pacific Ocean. Time lags in years are shown on top of each map for a lag-sequence from −10 to 10 years with a time step of 2 years. Positive lags mean SodSSHA lead regional sea level at Midway. The SodSSHA used here are for the upper 5–918 m of the ocean and for the period 1950–2007. A 10 year running mean filter was finally applied to the detrended data. Small green dots represent the regions where the cross correlations are statistically significant at ≥80% confidence level using the method of *Davis* [1976].

applied an empirical orthogonal function (EOF) analysis to RecSSHA updated for the period 1950–2009, AltSSHA and SodSSHA to estimate the regional response of sea level to IPO and compare the three data sets. The time-series were filtered with a 5 year low-pass Butterworth-filter to take full advantage of the higher resolution of the relatively short altimeter data set.

3. Results

3.1. Regional Sea Level at Key Locations

Estimates of 10 year running mean SodSSHA agree well with regional sea level estimates from the tide gauge data (Figures 1b and 1c). Correlation coefficients (R) between regional sea level observed at the Midway Island tide gauge (Midway hereafter) and SodSSHA at depths between 318 and 918 m ranged from 0.81 to 0.84, significant at >95% and 97% level, respectively. SODA captures the essential features of regional sea level including the decrease from 1950 to 1980 and the increase from 1980 to 2003. The secondary relative maximum from 1960 to 1966 and decrease after 2003 are also captured (Figure 1b). The decadal signal at Fremantle is smaller in amplitude but still reasonably well represented by SODA. The correlations clearly improve with contributions from increasing the depth-integrations ranging from 0.53 (to 318 m) to 0.76 (to 918 m) significant at >98.5% and 99.5% level, respectively (Figure 1c). This behavior was opposite at Midway, where correlation coefficients had a much smaller range across the depth. In addition, we found that the sea level at Midway and Fremantle is good indicator of changes in the IPO and PDO as they show significant anticorrelation with those indices. The correlation coefficients of the IPO and PDO with Midway are −0.76 and −0.68, and with Fremantle are −0.86 and −0.85, respectively.

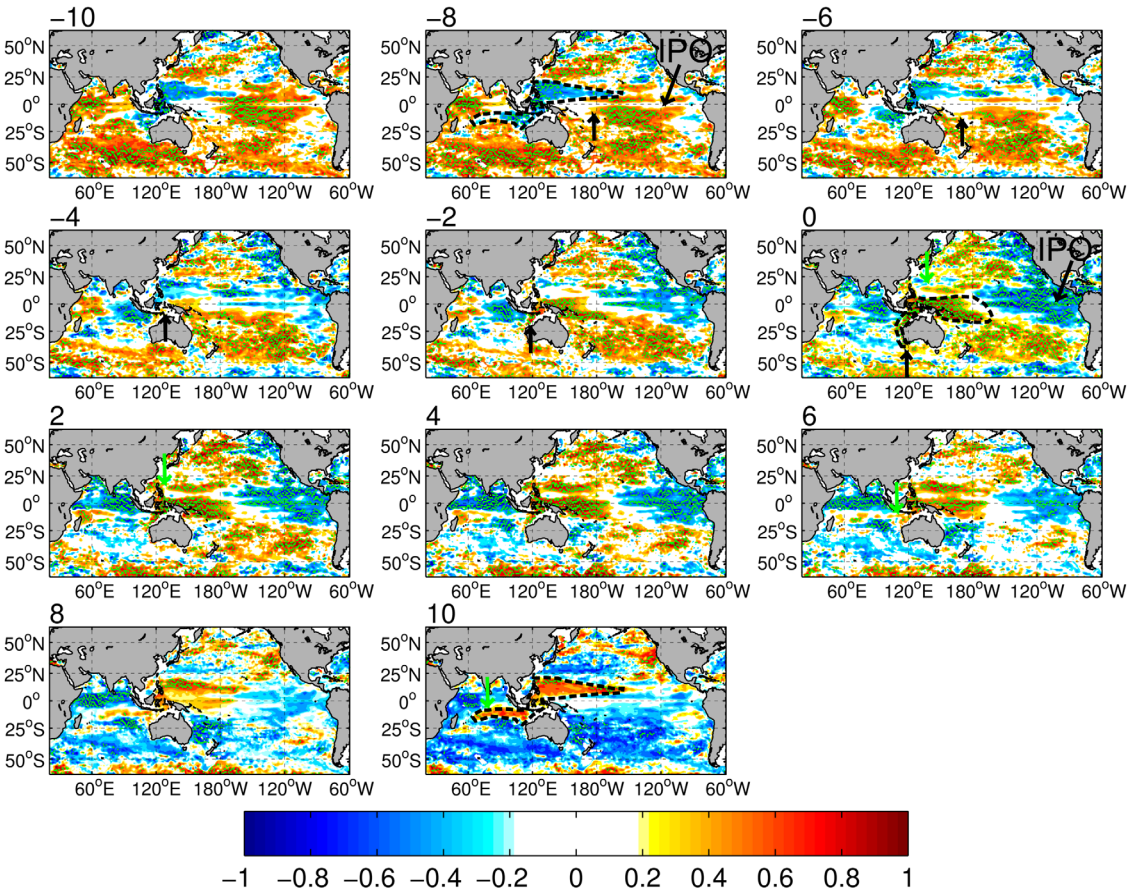

Figure 3. Spatial distribution of lagged-correlation coefficients (R) between regional sea level at Fremantle tide gauge and sea surface heights anomalies from SODA (SodSSHA) in the Indo-Pacific Ocean. Time lags in years are shown on top of each map for a lag-sequence from −10 to 10 years with a time step of 2 years. Positive lags mean SodSSHA lead regional sea level at Fremantle. The SodSSHA used here is for the upper 5–918 m of the ocean and for the period 1950–2007. A 10 year running mean filter was finally applied to the detrended data. Small green dots represent the regions where the cross correlations are statistically significant at ≥80% confidence level using the method of *Davis* [1976].

3.2. Spatial Correlation Analysis

A lagged (cross) correlation analysis was applied here to assess how SodSSHA at each spatial point compares to regional sea level at the tide gauges at different time lags. The analysis shows the spatial/temporal evolution of SodSSHA in the Indo-Pacific region as it relates to the regional variation. In particular, the spatial distribution and annual lag sequence (−10 to +10 years) between SodSSHA and Midway regional sea level shows important changes in the western and eastern Pacific Ocean (Figure 2). Green dots on the maps of sections 3.3 and 3.4 highlight the patterns that are significant at ≥80% confidence level using method of the *Davis* [1976], which takes account of the effective number of degrees of freedom due to serial correlation in the time series. There is a dominance of positive correlation coefficients across all lags in the northwest Pacific Ocean near the location of the tide gauge. The zero-lag pattern begins to develop 10 years earlier near 25°N then gradually spreads throughout the northwestern Pacific. The western tropical North Pacific Ocean (in particular near the Intertropical Convergence Zone) and tropical Indian Ocean are negatively correlated and seem to be connected via the Indonesian Seas from lag −10 to 0 (indicated by the dashed black contour in Figure 2). The negative correlation spreads throughout the tropical Indian Ocean by lag +10. Positive correlation coefficients in the eastern Pacific Ocean have an IPO-like pattern. Features with these positive correlation coefficients appear to move from the eastern Pacific Ocean to the western tropical South Pacific Ocean from lag −10 to 0 and penetrate into the Indonesian Seas and Western Australia coast along the coastal waveguide from lag +2 to +10 (indicated by black arrows in Figure 2). Negative correlation coefficients in the eastern Pacific Ocean appear at lag −2 and strengthen from lag 0 to +10, ending up with a negative pattern in the eastern Pacific Ocean. The area of negative phase is again reminiscent of the IPO pattern in SST.

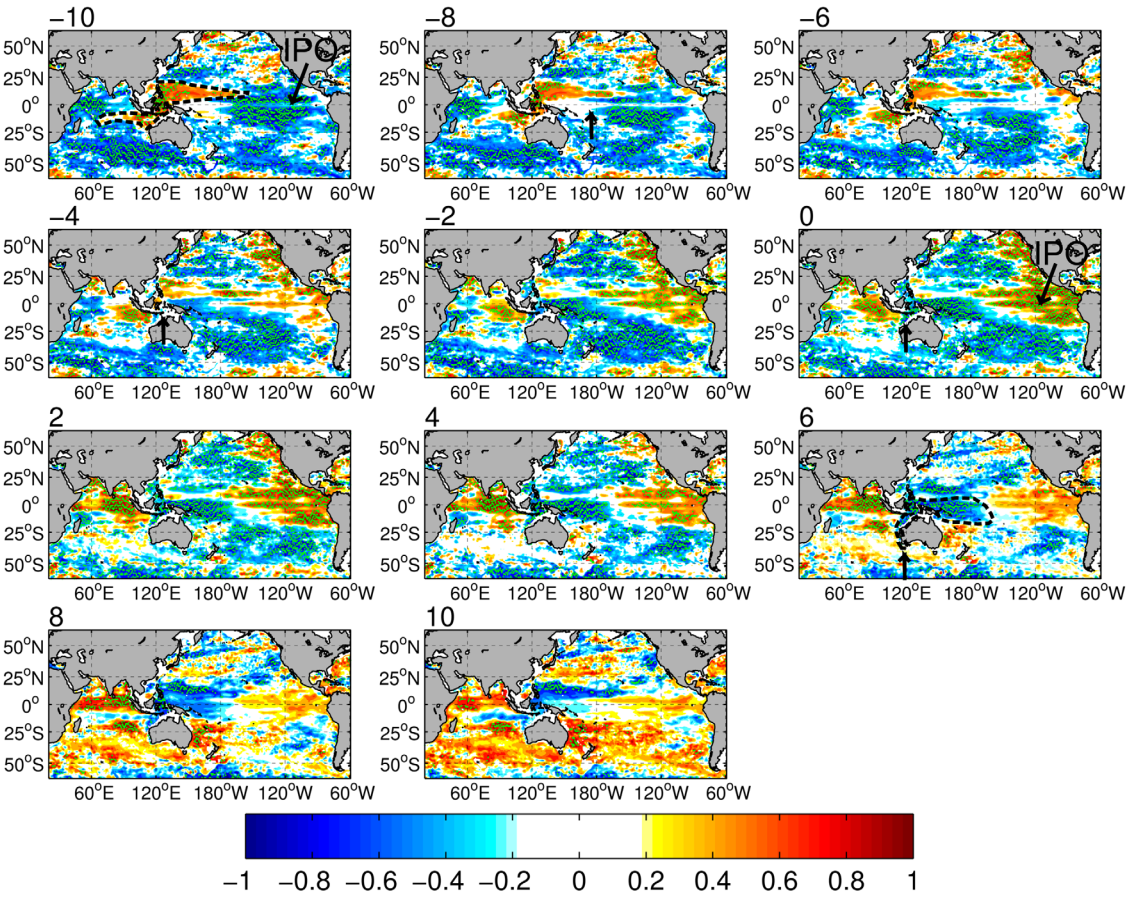

Figure 4. Spatial distribution of lagged-correlation coefficients (R) of sea surface heights anomalies from SODA (SodSSHA) and the IPO index in the Indo-Pacific Ocean. Time lags in years are shown on top of each map for a lag-sequence from −10 to 10 years with a time step of 2 years. Positive lags mean that the IPO index leads SodSSHA. The SodSSHA used here is for the upper 5–918 m of the ocean and for the period 1950–2007. A 10 year running mean filter was finally applied to the detrended data. Small green dots represent the regions where the cross correlations are statistically significant at ≥80% confidence level using the method of *Davis* [1976].

A similar analysis between the SodSSHA and Fremantle tide gauge regional sea level data also shows a clear evolution over time and space of an IPO-like pattern from lag −10 to +6 (Figure 3). Fremantle sea level is negatively correlated with SODA in the western tropical North Pacific Ocean, Indonesian Seas, and eastern tropical South Indian Ocean connected through the Indonesian Seas from lag −10 to −4. Patterns with positive correlation coefficients spread from the eastern Pacific Ocean to the western tropical South Pacific Ocean. These patterns appear to reach the Indonesian Seas and the coast of Western Australia along the waveguide from lag −10 to 0 (indicated by black arrows in Figure 3). Furthermore, positive correlation coefficients connect the western tropical North Pacific Ocean with the Indonesian Seas and the tropical South Indian Ocean from lag 0 to +10 (indicated by green arrows and black dashed contour in Figure 3). The transmission of interannual signals from the western tropical Pacific Ocean into the Indian Ocean has been noted in earlier studies and is associated with Rossby waves [*Meyers*, 1996; *Wijffels and Meyers*, 2004; *Cai et al*., 2005; *Alory et al*., 2007]; however, further analysis of the mechanism is needed considering the long time scale of the IPO.

In summary, both Midway (Figure 2) and Fremantle (Figure 3) tide gauges characterize the connections between the western tropical Pacific Ocean and Indian Ocean, each one emphasizing characteristics closely related to the location of the tide gauges. Hence, the regional sea level from both tide gauges is an excellent proxy for the connectivity on decadal time scales between the western tropical Pacific and the eastern tropical South Indian Ocean. Figures 1–3 show that the SODA sea level product is representative of regional sea level variation. It produces spatial patterns of temporal variation at decadal and longer time scales that are dynamically consistent with what is known from earlier studies.

3.3. IPO Connections

A lagged-correlation analysis between SodSSHA and the IPO index for several time lags shows a meridional asymmetry in the dynamic connections between the western tropical Pacific Ocean and the Indian Ocean which is presumably related to large-scale IPO changes (Figure 4). The asymmetry is highlighted at lags −10 and +6. This meridional asymmetry has in its northern side a pattern with positive correlations that connect the western tropical North Pacific Ocean (east of Borneo and the Philippine Islands) with the tropical South Indian Ocean (in a band out to 65°E) from lag −10 to −6 (Figure 4). The southern side of this asymmetry is characterized by a dynamic connection between the western tropical South Pacific Ocean (north of Papua New Guinea) and the eastern South Indian Ocean, apparently as a subsequent response of the preceding IPO event in the eastern Pacific Ocean. This connection follows the coastal waveguide along the coast of Western Australia from lag −2 to +6 (Figure 4). This spatial pattern develops in time and seems to spread on decadal time scales but not in a way consistent with simple free linear Rossby and Kelvin waves, since planetary wave processes would have to be much faster than 10 years in low latitudes. This meridional asymmetry can also be observed in the lagged-correlation analysis with the tide gauges in section 3.3 (Figures 2 and 3).

The paths of those dynamic connections between the western tropical Pacific Ocean and the South Indian Ocean seems to be related to changes of the IPO-like pattern in the eastern Pacific Ocean. For example, an IPO-like feature in the eastern Pacific Ocean, shown by negative correlation coefficients from lags −10 to −8, switched into positive values from lags −6 to +6, reaching a well-developed classic IPO pattern at lag 0. While these changes occur in the eastern Pacific Ocean, simultaneously features with negative correlation coefficients spread from the central Pacific Ocean to the western tropical South Pacific Ocean from lags −8 to −4 (indicated with black arrows in Figure 4). These negatively correlated features finally reach the southeast Indian Ocean along the coastal waveguide of Western Australia at lag +6 (Figure 4).

A similar meridional asymmetry was also identified by correlating temperature anomalies at thermocline depths (112 and 149 m depth) with the IPO index (not shown here as the results show the same phenomenon as that depicted in Figure 4). Most of the patterns discussed here are significant at ≥80% level using the method of *Davis* [1976] for all time lags (see green dots in Figures 2–4). Specifically, the dynamic connection between the western tropical South Pacific Ocean and the South Indian Ocean along the coast of Western Australia is also significant at >95% level but only from lag 0 to +2. On the other hand, the patterns connecting the western tropical North Pacific Ocean and the tropical South Indian Ocean (in a band out to 65°E) are significant until a maximum of 90% level.

The lagged-correlation analysis was also applied to the 5 year running mean filtered and detrended data (not shown here) and the results were similar to those using a low-pass filter with a 10 year cut-off. Hence, the number of degrees of freedom by low-pass filtering the data with a 10 year cut-off do not affect the interpretation of the correlation coefficients on decadal time scales. The ability of SODA to capture IPO-like patterns and dynamic connections between the western Pacific Ocean and the South Indian Ocean provides more confidence in using SODA for dynamical studies at decadal times scales in the Indo-Pacific Ocean.

3.4. Regression Analysis

Linear regression of SODA temperature anomalies at various depths (surface, 110 m, 230 m) across the entire domain against the IPO index shows patterns at the surface (Figure 5) consistent with our understanding of the IPO mode in SSTA discussed in the literature [*Folland et al*., 1999; *Power et al*., 1999b]. The interest here, however, is in the subsurface signature. At 112 m depth (Figure 5b), the analysis demonstrates that the dominant decadal mode of Pacific Ocean variability is also manifested through the base of the mixed layer and into the upper thermocline with negligible loss of amplitude. Interestingly, the classic IPO signature in the ocean temperature anomaly pattern is also very evident even at 229 m depth, albeit that the amplitudes of the anomalies are lower in magnitude (Figure 5c). For instance, a strong signal of the IPO is still found at 229 m depth in the southwest Equatorial Pacific (Figure 5c). Hence, the most prominent difference between the subsurface IPO and the known surface IPO pattern is observed in the western tropical Pacific Ocean where the anomalies are very strong (Figures 5b and 5c). These subsurface anomalies in the western tropical Pacific Ocean are connected with those in the eastern South Indian Ocean through the Indonesian Seas and Western Australia coast.

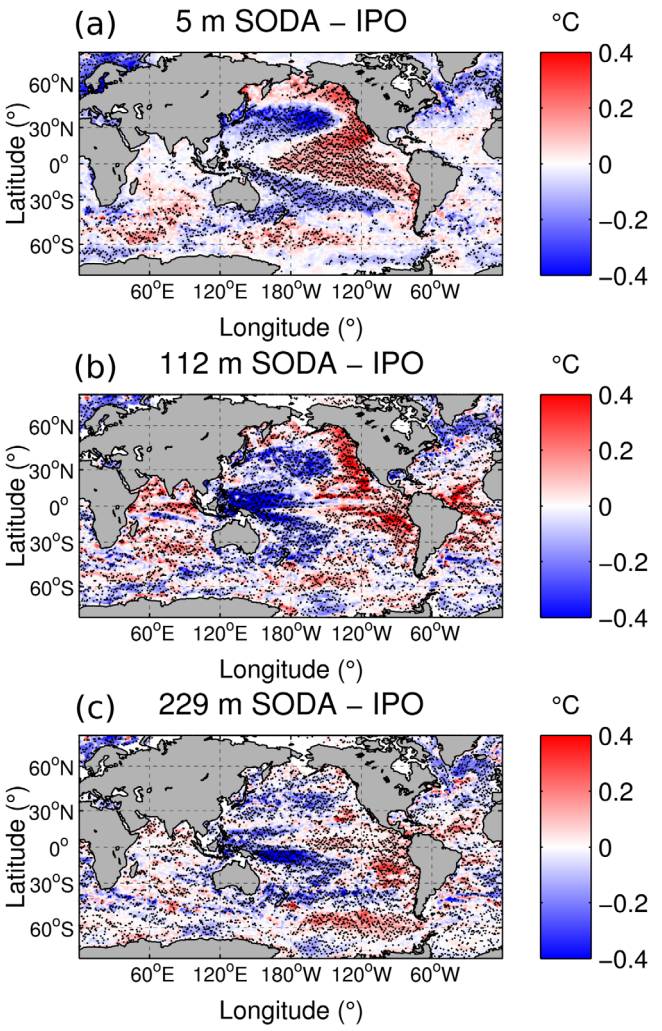

Figure 5. Linear regression of SODA temperatures onto the IPO index across various vertical levels including (a) sea surface, (b) 112 m depth, and (c) 229 m depth. Small black dots represent the regions where the regression coefficients are statistically significant at ≥95% confidence level using the method of *Davis* [1976].

3.5. Vertical Expression of Decadal Variability

Meridionally averaged ocean temperature anomalies, as a function of time and longitude, were examined at 50 m increments through the ocean's vertical structure down to 300 m depth (Figure 6). Four regions of the Indo-Pacific were examined here. This was undertaken to further explore how the IPO/PDO-related temperature variability extends from surface to subsurface in the Pacific Ocean and possibly connects into the Indian Ocean. The North Pacific Ocean, which is explicitly characterized by the PDO as its dominant decadal mode [*Mantua et al.*, 1997], provides a good example of how decadal variability extends through the upper ocean and into the thermocline (Figure 6a). Here the upper 200 m of the North Pacific shows strong decadal variability with similar intensity patterns as at the surface, but with reduced amplitude at 300 m depth.

The tropical Pacific Ocean region is characterized by the strongest decadal variability through the base of the mixed layer and upper thermocline at around 100–200 m depth (Figure 6b). This strong signal in the subsurface decadal variability is transmitted as anomalies from the western tropical Pacific Ocean into the South Indian Ocean, as described in sections 3.3 and 3.4.

The decadal scale subsurface temperature anomalies of the South Pacific Ocean show decadal variability that intensifies over the vertical structure and is strongest in the eastern South Pacific Ocean (Figure 6c). In particular, the strongest decadal variability patterns appear around 80°W in the eastern South Pacific Ocean and extend westward around 110°W at deeper vertical levels.

The largest temperature anomaly signal expressed in the tropical South Indian Ocean region occurs in the upper thermocline with decadal westward signals evident between 100–300 m (Figure 6d). These signatures within the thermocline have similar magnitude to those identified in the western tropical Pacific Ocean (see Figure 6b) again suggesting a possible connection of these anomalies between the Pacific and Indian Ocean basins.

To provide a clearer image of the vertical expression of decadal variability in the tropical Pacific Ocean as shown in Figure 6b, temperature anomalies for two averaged boxes along the western and eastern tropical Pacific Ocean were also calculated (Figure 7). We found that in SODA the western tropical Pacific Ocean shows more intense subsurface decadal variability with a deeper vertical expression (Figure 7a) than in the eastern tropical Pacific Ocean (Figure 7b). The decadal variability at thermocline depths in the western and eastern tropical Pacific Ocean also show opposite signs particularly from 1970s onward. This matches with the spatial patterns of temperature anomalies in the upper thermocline characterized in the regression

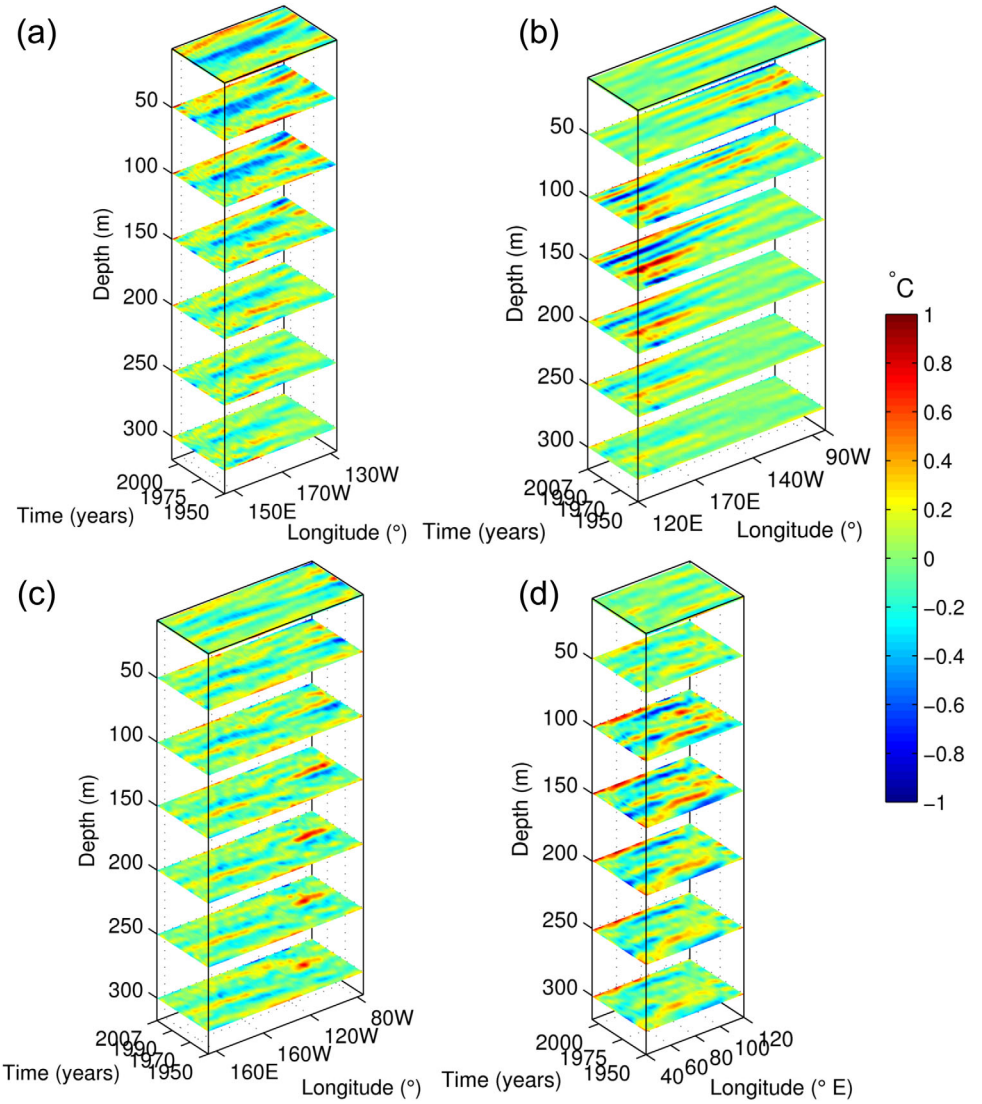

Figure 6. Time evolution of SODA temperature anomalies (at depth levels) against longitude for a meridional-averaged band in the (a) North Pacific Ocean (30.25°N–50.25°N), (b) tropical Pacific Ocean (12.25°S–12.25°N), (c) South Pacific Ocean (15.25°S–30.25°S), and (d) tropical South Indian Ocean (9.25°S–19.25°S). Temperature data were detrended and 10 year low-passed Butterworth-filtered.

analysis (Figure 5b) that shows a west-east dipole related to the IPO signature along the thermocline in the tropical Pacific Ocean.

3.6. EOF Analysis of SODA and Reconstructed Sea Level Data

Using a comparative EOF analysis of the decadally filtered SodSSHA and RecSSHA data sets, we find that the spatial pattern and time signature of EOF1 (56% of the variance) of RecSSHA and EOF2 (15% of the variance) of SodSSHA match well (compare spatial patterns of the modes shown in Figures 8a and 8c, and the temporal relationship between the corresponding PCs shown in Figure 8e). While there are clear similarities between these data sets in both space and time at the decadal scale, we nevertheless note that RecSSHA (Figure 8c) has larger spatial loadings than SODA in the eastern equatorial Pacific (Figure 8a). The EOF time series (PCs) are strongly correlated ($R = 0.85$, significant at $>99.9\%$ level, Figure 8e) and show highly similar decadal fluctuations. The similarity between the mode patterns and timing gives us substantial confidence in the SODA results. Nevertheless, we note the different ordering of the modes for this decadal-scale ocean climate signature between SODA (EOF2) and RecSSHA (EOF1) with substantially different variances explained. We are not too concerned about this because these differences are almost

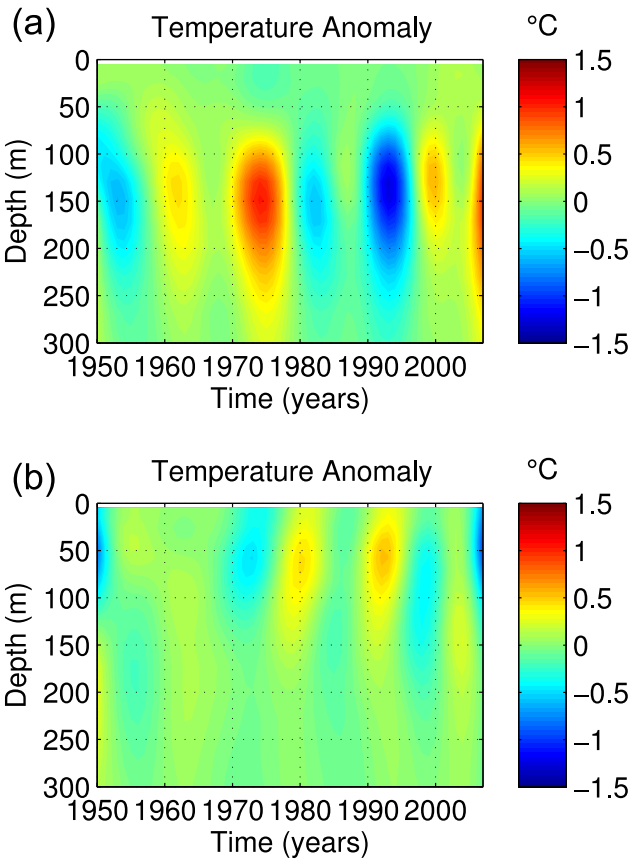

Figure 7. SODA temperature anomalies as a function of depth and time for an averaged box in the (a) western tropical Pacific Ocean (12.25°N–12.25°S, 120.25°E–179.75°E) and (b) eastern tropical Pacific Ocean (12.25°N–12.25°S, 179.75°E–80.25°W). Figures 7a and 7b match with the western and eastern sides of Figure 6b, respectively. Temperature data were detrended and 10 year low-passed Butterworth-filtered.

certainly related to the stronger multidecadal variability in SODA than in the RecSSHA which makes the variance distribution in SODA more spread among several modes.

EOF1 of SodSSHA explains 20% of the total variance (Figure 9a) and its PC is dominated by multidecadal fluctuations (Figure 9c). EOF1 and EOF2 of SodSSHA represent a couplet, according to the *North et al.* [1982] test; however, EOF1 is not correlated with the IPO index (Figure 9c). EOF1 and EOF2 of SodSSHA may be the quadrature constructs of the IPO (i.e., not independent standing patterns). Interestingly, EOF1 of SodSSHA (Figure 9a) shows a spatial pattern that appears to connect the western tropical North Pacific Ocean with the tropical South Indian Ocean. This pattern is similar to that derived by the lagged-correlation analysis in sections 3.3 and 3.4; and its associated PC (Figure 9c) shows multidecadal variability, suggesting that this dynamic connection might be multidecadal in nature. But why does RecSSHA not show multidecadal variability like that corresponding to EOF1 of SodSSHA? One possible explanation could be that RecSSHA includes only tide gauge data before 1993 with sparse spatial distribution prior to the satellite era and thus insufficient to attribute substantial variance to the description of large scale patterns of multidecadal variability. Nevertheless, the RecSSHA represents well the decadal variability which is the main interest here.

EOF1 of AltSSHA (49% of the variance) and SodSSHA (39% of the variance) are also in very good agreement in space (cf. Figures 8b and 8d) and time (Figure 8f), with the EOF time series (PCs) correlating strongly ($R = 0.96$, significant at $>99.5\%$ level). We found that the PCs of SodSSHA correlate well with the IPO index on both the long ($R = 0.87$, $>99.9\%$ significance, 1950–2007) and shorter time scales ($R = 0.89$, significant at $>99\%$ level, 1993–2007). Hence, these modes appear to characterize the IPO, identified in EOF2 in SODA for the period 1950–2007 but in EOF1 for the period 1993–2007. Characteristically, the RecSSHA (period 1950–2007) and AltSSHA data sets (period 1993–2007) also identify the IPO signature in EOF1. In short, EOF1 of AltSSHA and SodSSHA for the period 1993–2007 explains almost the same amount of variance and neither of them capture multidecadal variability as observed in SodSSHA for the period 1950–2007.

The same procedure as above was also performed on the annual (not filtered) and detrended SSHA (not shown here) using the three data sets. The results were found to be very similar, but the spatial patterns tended to be more equatorial in focus, and appears as EOF1 in both the SodSSHA and RecSSHA data sets for the period 1950–2007 ($R = 0.82$, $>99.9\%$ significance). For the unfiltered case, the leading modes of SodSSHA and the AltSSHA for the period 1993–2007 also agree well in space and time ($R = 0.73$, $>99.5\%$ significance).

4. Summary and Discussion

This paper has evaluated SODA 2.2.4 against independent sea level anomaly observations from tide gauge, satellite altimeters, and reconstructed data. Our analysis shows that regional sea level from SODA is clearly

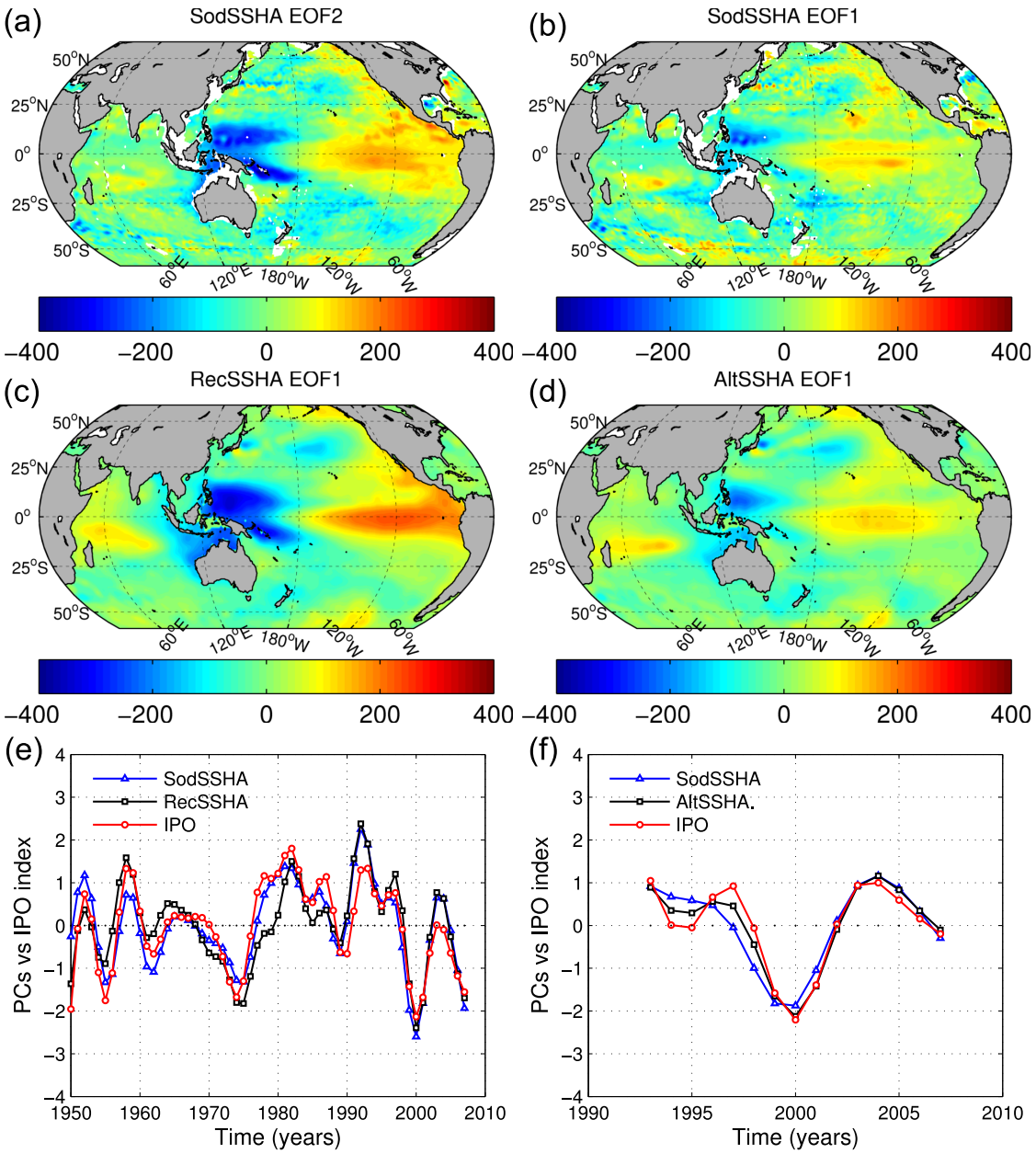

Figure 8. (a) EOF2 (1950–2007) and (b) EOF1 (1993–2007) of SSHA from SODA (SodSSHA), and EOF1 of the (c) reconstructed SSHA as outlined by *Church et al.* [2004] (RecSSHA, 1950–2007), and (d) SSHA from altimeter data (AltSSHA, 1993–2007). (e and f) The principal components (PCs) of the modes and the IPO index. The data have been detrended and a 5 year low-pass Butterworth-filter have been applied. The PCs (Figures 8e and 8f) and the IPO index have been standardized for visual purposes.

related to the IPO signals observed in sea level at the Midway Island and the Fremantle tide gauges. We find that Midway Island sea level varies coherently with the IPO and PDO indices and is an ideal center for Pacific Ocean decadal studies of sea level.

There appears to be a meridional asymmetry in the dynamic connection between the tropical Pacific Ocean and the Indian Ocean apparently as a response to changes in the large scale evolution of the IPO. The asymmetry is seen in Figure 2, the lagged correlation of sea level at Midway with SodSSHA, and in Figure 10, a schematic of the asymmetry. The lagged-correlation analysis shows that the important connection between the western North Pacific Ocean and tropical South Indian Ocean (Figures 2 and 10a) corresponds to the IPO signal at Midway lagging SodSSHA in the lag sequence period from −10 to −6 years (Figure 2). The connection between the western South Pacific Ocean and eastern South Indian Ocean in the coastal

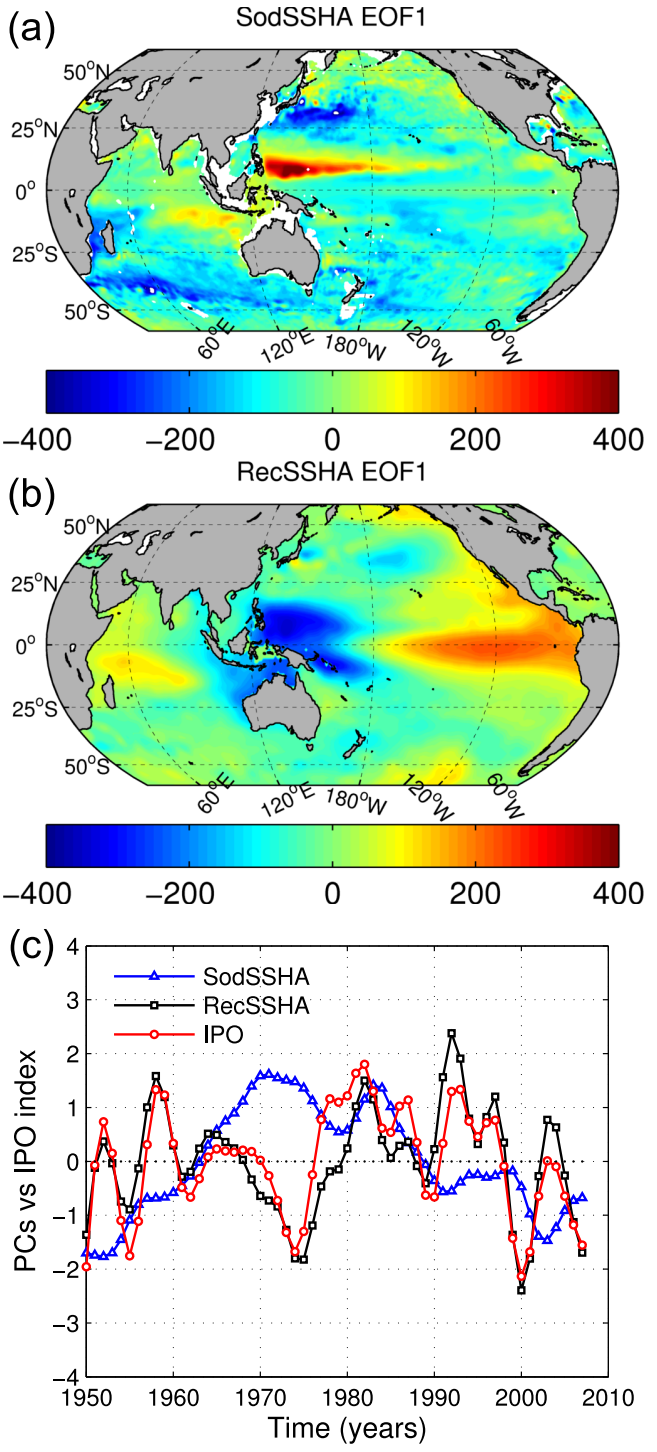

Figure 9. EOF1 (1950–2007) of SSHA from (a) SODA (SodSSHA) and (b) reconstructed SSHA as outlined by *Church et al.* [2004] (RecSSHA). (c) The principal components (PCs) and the IPO index, which have been standardized for visual purposes. The data have been detrended and a 5 year low-pass Butterworth-filter have been applied.

waveguide off Western Australia (Figures 2 and 10b) corresponds to the IPO signal at Midway leading SodSSHA in the lag sequence period from −2 to +6 years (Figure 2). Stated another way, SodSSHA spreads westward into the tropical Indian Ocean before the IPO at Midway reaches an extremum. The lead lag relationships identified here are relevant to efforts to develop the capability for decadal prediction.

We have demonstrated that SODA is representative of the thermal structure of the Indo-Pacific Ocean during cycles of IPO/PDO. The connection (for example lag −10 in Figures 4 and 9a) between the Indian Ocean and the western tropical Pacific Ocean found here, as a response to changes in the IPO, might be related to the multidecadal connectivity via ocean-atmosphere interactions between these two ocean basins suggested by *Luo et al.* [2012] who find that stronger (weaker) Indian Ocean warming, relative to the Pacific's, helps to enhance (weaken) the Pacific trade winds by modulating the Walker circulation. Two papers to be submitted will use the SODA product to analyze connectivity on decadal to multidecadal time scales between the Pacific and Indian Oceans.

We also found that by linearly regressing each spatial point time series of temperature from SODA over the Indo-Pacific Ocean domain onto the IPO index, the IPO mode in SST as reported in the literature is well reproduced [*Folland et al.*, 1999; *Power et al.*, 1999b]. The regression applied to the subsurface also indicates that the IPO signature extends through the upper ocean including through the mixed layer and upper thermocline, thus highlighting the IPO's importance in upper ocean dynamics consistent with previous modeling studies and discussions by, for example, *McGregor et al.* [2004] and *Power and Colman* [2006]. We conclude that the IPO is well described by SODA and it is not only a feature at the sea surface but extends through the upper 200–300 m to thermocline depths across the Pacific Ocean and possibly the eastern South Indian Ocean.

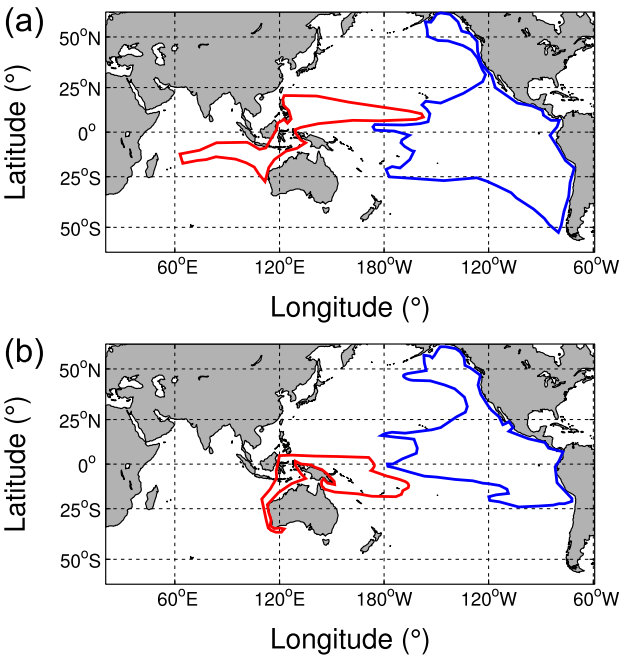

Figure 10. Schematic representation of the spatial patterns associated with the dynamic connections between the western tropical Pacific Ocean and the South Indian Ocean via the Indonesian Seas at decadal time scales. Figure 10a represents the connection between the western tropical North Pacific Ocean and the tropical South Indian Ocean via the Indonesian Seas. Figure 10b represents the connection between the western tropical South Pacific Ocean and the coast of Western Australia via Indonesian Seas. This interpretation is based on the analysis of the spatial distribution of lagged-correlation analysis using regional sea level from tide gauges, IPO index, and sea surface height anomalies (5–918 m) from SODA. These two patterns in the western tropical Pacific Ocean are meridionally asymmetric. Red and blue lines symbolize that the phases are opposite; however, the pattern along the western tropical North Pacific and the pattern along the western tropical South Pacific Ocean occur at different times during the IPO cycle.

Subsurface IPO features are different from those at the sea surface, particularly in the western tropical Pacific Ocean where the anomalies are stronger at the subsurface than at the surface. Those subsurface anomalies also indicate that the western tropical Pacific and the eastern South Indian Ocean are connected through the Indonesian Seas and Western Australia coast. This supports the dynamic connection between the tropical western Pacific Ocean and the eastern South Indian Ocean highlighted in the spatial lagged-correlation analysis between SodSSHA and sea level from tide gauges (and IPO index).

We have also shown that SODA reproduces well the low-frequency (decadal) variability of SSHA observed in the reconstructed (RecSSHA) data set from *Church et al*. [2004] (updated for the period 1950–2009). Both data sets describe similar decadal scale SSHA patterns and time signatures, and more specifically that are highly correlated with the large scale IPO—although we caveat that the RecSSHA relies on tide gauge records prior to 1993 and is conditioned on satellite information since 1993. Interestingly, the decadally filtered EOF1 of SodSSHA captures the multidecadal variability, but is not featured in the dominant modes of RecSSHA from *Church et al*. [2004]. In short, we find that the RecSSHA record is a useful tool to evaluate SODA on decadal time scales, although it has to be used with caution on multidecadal time scales.

EOF analysis on the SodSSHA for the period 1993–2007 against AltSSHA further highlights the integrity of SODA at the decadal scale. The AltSSHA are homogeneous and much higher resolution observations in space and time than the RecSSHA. The EOF1 time series from this shorter record analysis are also significantly correlated with the IPO index. We note that SODA captures the same interannual variability estimated in RecSSHA—which has a strong El Niño-Southern Oscillation signature in SSHA and SSTA compared with numerous previous studies [e.g., *Church et al*., 2004; *Church and White*, 2011].

The differences between the spatial patterns of EOF2 of SodSSHA (or RecSSHA) for the period 1950–2007 and EOF1 of SodSSHA (or AltSSHA) for the period 1993–2007 (Figure 8), both of which are consistent with the IPO pattern, are probably due to the phase change in the IPO from positive to negative since 1993 as discussed by *Han et al*. [2013] in sea surface temperature. *England et al*. [2014] explain that the most recent cooling in the tropical eastern Pacific Ocean is related to the strengthening of the trade winds and the negative IPO phase since 2001. The IPO "cold transition" in the period 1993–2007 is expressed as less intense variance in SodSSHA (small SodSSHA) than for the period 1950–2007 particularly in the eastern Pacific Ocean (Figure 8).

Based on our analysis and evaluation here, we find SODA to be a useful tool for investigating regional to large scale upper ocean decadal to multidecadal variability in temperature and sea level (quasi-steric component of sea level). SODA reproduces the decadal sea surface height signals observed in

long-term tide gauges at key locations for examining large scale ocean climate variability (Midway Island and Fremantle) while also characterizing the IPO through the vertical temperature structure for possible studies of IPO ocean dynamics. Our analysis further shows that SODA is robust enough to reproduce annual-to-decadal variability observed in independent observations from reconstructed sea level data from *Church et al.* [2004] and TOPEX/Poseidon satellite altimeter data, and therefore that this product provides a potentially useful model synthesis of the sparse historical observations in the upper ocean on decadal time scales.

Acknowledgments

This work was conducted as part of the José Mauro Vargas Hernández PhD in Quantitative Marine Sciences PhD Program, a joint initiative between the University of Tasmania and CSIRO. The research was partially supported by grants from University of Tasmania, Universidad Nacional de Costa Rica, and CSIRO. The authors are thankful to John Church and Neil White from CSIRO Marine and Atmospheric Research for providing sea level data at Midway Island and Fremantle, the reconstructed sea level for the period 1950–2009, and the TOPEX/Poseidon satellite altimeter data (data available from http://www.cmar.csiro.au/sealevel/index.html). Richard Coleman is thanked for suggesting the EOF analysis used to prepare Figure 8. SODA data were provided by the SODA/TAMU research group, Texas A&M University (http://soda.tamu.edu/). The dynamic height anomaly was estimated using the Gibbs Seawater (GSW) Oceanographic Toolbox of the Thermodynamic Equation of Seawater (TEOS-10) [*McDougall and Barker*, 2011] available from http://www.teos-10.org/. The IPO index was obtained from the calculations of Chris Folland, UK Met Office Hadley Centre (http://iges.org/c20c/IPO_v2.doc). The PDO index was obtained from the Joint Institute for the study of the Atmosphere and Ocean (JISAO) at University of Washington (http://jisao.washington.edu/pdo/). This paper makes a contribution to the goals of the Australian Research Council Centre of Excellence for Climate System Science.

References

Alory, G., S. Wijffels, and G. Meyers (2007), Observed temperature trends in the Indian Ocean over 1960–1999 and associated mechanisms, *Geophys. Res. Lett.*, *34*, L02606, doi:10.1029/2006GL028044.

Boyer, T., et al. (2009), *World Ocean Database 2009, NOAA Atlas NESDIS*, vol. 66, 216 pp., U.S. Govt. Print. Off., Washington, D. C.

Cai, W., G. Meyers, and G. Shi (2005), Transmission of ENSO signal to the Indian Ocean, *Geophys. Res. Lett.*, *32*, L05616, doi:10.1029/2004GL021736.

Carton, J., and B. Giese (2008), A reanalysis of ocean climate using Simple Ocean Data Assimilation (SODA), *Mon. Weather Rev.*, *136*(8), 2999–3017, doi:10.1175/2007MWR1978.1.

Church, J. A., and N. J. White (2011), Sea-level rise from the late 19th to the early 21st century, *Surv. Geophys.*, *32*(4–5), 585–602, doi:10.1007/s10712-011-9119-1.

Church, J. A., N. J. White, R. Coleman, K. Lambeck, and J. X. Mitrovica (2004), Estimates of the regional distribution of sea level rise over the 1950–2000 period, *J. Clim.*, *17*(13), 2609–2625, doi:10.1175/1520-0442(2004)017<2609:EOTRDO>2.0.CO;2.

Compo, G., et al. (2011), The twentieth century reanalysis project, *Q. J. R. Meteorol. Soc.*, *137*(654), 1–28, doi:10.1002/qj.776.

Corre, L., L. Terray, M. Balmaseda, A. Ribes, and A. Weaver (2012), Can oceanic reanalyses be used to assess recent anthropogenic changes and low-frequency internal variability of upper ocean temperature?, *Clim. Dyn.*, *38*, 877–896, doi:10.1007/s00382-010-0950-8.

Davis, J. L., and J. X. Mitrovica (1996), Glacial isostatic adjustment and the anomalous tide gauge record of eastern North America, *Nature*, *379*, 331–333, doi:10.1038/379331a0.

Davis, R. (1976), Predictability of sea surface temperature and sea level pressure anomalies over the North Pacific Ocean, *J. Phys. Oceanogr.*, *6*(3), 249–266, doi:10.1175/1520-0485(1976)006<0249:POSSTA>2.0.CO;2.

England, M. H., S. McGregor, P. Spence, G. A. Meehl, A. Timmermann, W. Cai, A. S. Gupta, M. J. McPhaden, A. Purich, and A. Santoso (2014), Recent intensification of wind-driven circulation in the Pacific and the ongoing warming hiatus, *Nat. Clim. Change*, *4*(3), 222–227, doi:10.1038/nclimate2106.

Feng, M., Y. Li, and G. Meyers (2004), Multidecadal variations of Fremantle sea level: Footprint of climate variability in the tropical Pacific, *Geophys. Res. Lett.*, *31*, L16302, doi:10.1029/2004GL019947.

Feng, M., M. McPhaden, and T. Lee (2010), Decadal variability of the Pacific subtropical cells and their influence on the southeast Indian Ocean, *Geophys. Res. Lett.*, *37*, L09606, doi:10.1029/2010GL042796.

Folland, C., D. Parker, A. Colman, and R. Washington (1999), *Large Scale Modes of Ocean Surface Temperature Since the Late Nineteenth Century*, chap. 4, pp. 73–102, Springer, Berlin, doi:10.1007/978-3-642-58369-8-4.

Giese, B. S., and S. Ray (2011), El Niño variability in Simple Ocean Data Assimilation (SODA), 1871–2008, *J. Geophys. Res.*, *116*, C02024, doi:10.1029/2010JC006695.

Han, W., et al. (2013), Intensification of decadal and multi-decadal sea level variability in the western tropical Pacific during recent decades, *Clim. Dyn.*, *1–23*, doi:10.1007/s00382-013-1951-1.

Holbrook, N. J., I. D. Goodwin, S. McGregor, E. Molina, and S. B. Power (2011), ENSO to multi-decadal time scale changes in East Australian Current transports and Fort Denison sea level: Oceanic Rossby waves as the connecting mechanism, *Deep Sea Res., Part II*, *58*(5), 547–558, doi:10.1016/j.dsr2.2010.06.007.

Levitus, S., J. Antonov, T. Boyer, R. Locarnini, H. Garcia, and A. Mishonov (2009), Global ocean heat content 1955–2008 in light of recently revealed instrumentation problems, *Geophys. Res. Lett.*, *36*, L07608, doi:10.1029/2008GL037155.

Luo, J.-J., W. Sasaki, and Y. Masumoto (2012), Indian Ocean warming modulates Pacific climate change, *Proc. Natl. Acad. Sci. U. S. A.*, *109*(46), 18,701–18,706, doi:10.1073/pnas.1210239109.

Mantua, N., S. Hare, Y. Zhang, J. Wallace, and R. Francis (1997), A Pacific interdecadal climate oscillation with impacts on salmon production, *Bull. Am. Meteorol. Soc.*, *78*(6), 1069–1079, doi:10.1175/1520-0477(1997)078<1069:APICOW>2.0.CO;2.

McCabe, G., M. Palecki, and J. Betancourt (2004), Pacific and Atlantic Ocean influences on multidecadal drought frequency in the United States, *Proc. Natl. Acad. Sci. U. S. A.*, *101*(12), 4136–4141, doi:10.1073/pnas.0306738101.

McDougall, T. J. and P. M. Barker (2011), *Getting Started With TEOS-10 and the Gibbs Seawater (GSW) Oceanographic Toolbox*, vol. 7, 28 pp., SCOR/IAPSO WG127.

McGregor, S., N. J. Holbrook, and S. B. Power (2004), On the dynamics of interdecadal thermocline depth and sea surface temperature variability in the low to mid-latitude Pacific Ocean, *Geophys. Res. Lett.*, *31*, L24201, doi:10.1029/2004GL021241.

Meinke, H., P. DeVoil, G. L. Hammer, S. Power, R. Allan, R. C. Stone, C. Folland, and A. Potgieter (2005), Rainfall variability at decadal and longer time scales: Signal or noise?, *J. Clim.*, *18*(1), 89–96, doi:10.1175/JCLI-3263.1.

Meyers, G. (1996), Variation of Indonesian throughflow and the El Niño-Southern Oscillation, *J. Geophys. Res.*, *101*(C5), 12,255–12,263, doi:10.1029/95JC03729.

Milne, G., J. Davis, J. X. Mitrovica, H.-G. Scherneck, J. Johansson, M. Vermeer, and H. Koivula (2001), Space-geodetic constraints on glacial isostatic adjustment in Fennoscandia, *Science*, *291*(5512), 2381–2385, doi:10.1126/science.1057022.

North, G. R., T. L. Bell, R. F. Cahalan, and F. J. Moeng (1982), Sampling errors in the estimation of empirical orthogonal functions, *Mon. Weather Rev.*, *110*(7), 699–706, doi:10.1175/1520-0493(1982)110<0699:SEITEO>2.0.CO;2.

Power, S., and R. Colman (2006), Multi-year predictability in a coupled general circulation model, *Clim. Dyn.*, *26*(2–3), 247–272, doi:10.1007/s00382-005-0055-y.

Power, S., F. Tseitkin, V. Mehta, B. Lavery, S. Torok, and N. Holbrook (1999a), Decadal climate variability in Australia during the twentieth century, *Int. J. Climatol.*, *19*(2), 169–184, doi:10.1002/(SICI)1097-0088(199902)19:2<169::AID-JOC356>3.0.CO;2-Y.

Power, S., T. Casey, C. Folland, A. Colman, and V. Mehta (1999b), Inter-decadal modulation of the impact of ENSO on Australia, *Clim. Dyn.*, *15*(5), 319–324, doi:10.1007/s003820050284.

Smith, R., et al. (2010), The Parallel Ocean Program (POP) reference manual: Ocean component of the Community Climate System Model (CCSM), *Tech. Rep. LAUR-10-01853*, Los Alamos Natl. Lab., Los Alamos, N. M.

Ummenhofer, C. C., M. H. England, P. C. McIntosh, G. A. Meyers, M. J. Pook, J. S. Risbey, A. S. Gupta, and A. S. Taschetto (2009), What causes southeast Australia's worst droughts?, *Geophys. Res. Lett.*, *36*, L04706, doi:10.1029/2008GL036801.

Wijffels, S., and G. Meyers (2004), An intersection of oceanic waveguides: Variability in the Indonesian throughflow region, *J. Phys. Oceanogr.*, *34*(5), 1232–1253.

Wijffels, S., J. Willis, C. Domingues, P. Barker, N. White, A. Gronell, K. Ridgway, and J. Church (2008), Changing expendable bathythermograph fall rates and their impact on estimates of thermosteric sea level rise, *J. Clim.*, *21*(21), 5657–5672, doi:10.1175/2008JCLI2290.1.

Woodruff, S. D., et al. (2010), ICOADS Release 2.5: Extensions and enhancements to the surface marine meteorological archive, *Int. J. Climatol.*, *31*(7), 951–967, doi:10.1002/joc.2103.